1986

# Predicting Shunt Currents in Stacks of Bipolar Plate Cells

Ralph E. White
*University of South Carolina - Columbia*, white@cec.sc.edu

C. W. Walton
*Texas A & M University - College Station*

H. S. Burney

R. N. Beaver



## Publication Info

*Journal of the Electrochemical Society*, 1986, pages 485-492.

Publisher's Version:
http://dx.doi.org/10.1149/1.2108606
DOI: 10.1149/1.2108606

2. A. Amith, *J. Vac. Sci. Technol.*, **15**, 353 (1978).
3. K. Mitchell, A. L. Fahrenbruch, and R. H. Bube, *ibid.*, **12**, 909 (1975).
4. Y. Y. Ma and R. H. Bube, *This Journal*, **124**, 1430 (1977).
5. B. F. Shirreffs, C. H. Cheng, K. Geib, and K. A. Jones, *ibid.*, **131**, 440 (1984).
6. N. Nakayama, H. Matsumoto, A. Nakano, S. Ikegami, H. Uda, and T. Yamashita, *Jpn. J. Appl. Phys.*, **19**, 703 (1980).
7. H. Uda, H. Matsumoto, Y. Komatsu, A. Nakano, and S. Ikegami, in Proceedings of the 16th IEEE Photovoltaic Specialist Conf., San Diego, Sept. 1982, p. 801, IEEE, New York (1982).
8. H. Uda, H. Matsumoto, Y. Kuribayashi, Y. Komatsu, A. Nakano, and S. Ikegami, *Jpn. J. Appl. Phys.*, **22**, 1832 (1983).
9. J. S. Lee and H. B. Im, *J. Mater. Sci.*, Accepted for publication.
10. J. S. Lee, Y. K. Jun, and H. B. Im, To be published.
11. H. G. Yang and H. B. Im, *J. Mater. Sci.*, Accepted for publication.
12. P. L. Kukk and M. E. Altosaar, *J. Solid State Chem.*, **48**, 1 (1983).
13. H. T. Kim and H. B. Im, *IEEE Trans. Magn.*, **mag-18**, 1541 (1982).
14. N. Romeo, *J. Cryst. Growth*, **52**, 692 (1981).
15. J. Y. W. Seto, *J. Appl. Phys.*, **46**, 5247 (1975).
16. G. Baccarani, B. Ricco, and G. Spadini, *ibid.*, **49**, 5865 (1978).
17. J. W. Orton, B. J. Goldsmith, J. A. Chapman, and M. J. Powell, *ibid.*, **53**, 1602 (1982).
18. F. B. Micheletti and P. Mark, *Appl. Phys. Lett.*, **10**, 136 (1967).

# Predicting Shunt Currents in Stacks of Bipolar Plate Cells

**R. E. White* and C. W. Walton****

*Department of Chemical Engineering, Texas A&M University, College Station, Texas 77843*

**H. S. Burney and R. N. Beaver**

*Dow Chemical USA, Texas Applied Science and Technology Laboratories, Freeport, Texas 77541*

ABSTRACT

A method is presented for predicting shunt currents in stacks of undivided and divided bipolar plate cells. The method is an efficient way of solving the coupled sets of algebraic equations that arise from using circuit analog models to represent the current paths in stacks of undivided or divided bipolar plate cells. These algebraic equations can be either linear or nonlinear depending upon the current-potential relationships used in the model (*i.e.*, nonlinear circuit elements can be included). The method is used to show the importance of including nonsymmetrical resistances and nonlinear circuit elements in the models. Also, the method is used to predict the shunt currents for a nine cell stack of pilot plant scale bipolar plate, membrane chlor-alkali cells. It is shown that these predictions agree qualitatively with measured values. Finally, the method is used to predict the shunt currents for stacks of 60 and 120 of these cells.

*Undivided cells.*—It is well known that shunt currents exist in stacks of bipolar plate cells with common electrolytes, as shown schematically in Fig. 1. These shunt currents are undesirable for at least two reasons: they can cause corrosion of some of the components of the system, and they are currents that are essentially lost in terms of the production of the desired products of the system. The corrosion problem can be particularly severe if the shunt currents leave the cells via conducting nozzles to which are attached the inlet and outlet tubes for the cells. It is desirable, therefore, to be able to predict the shunt currents for all of the inlet and outlet tubes for cells in stacks, such as that shown in Fig. 1, to provide a means of predicting the "worst case" corrosion rates of the connecting nozzles. This is considered a worst case because the shunt currents in the tubes cannot be expected to appear entirely as the dissolution of the nozzle. It is, of course, also desirable to be able to predict the total amount of shunt current to provide a means of estimating the efficiency of the stack.

The shunt currents shown in Fig. 1 can be predicted by using a circuit analog model, as shown in Fig. 2 for N cells. This model is based on the conceptualization that the total current ($I_T$) enters the solution in the first cell through the terminal anode and then passes through one-half of a cell resistance ($R_e/2$). The total current can then either continue through the other half of the first cell resistance or split and leave the cell through the connecting channels (or tubes) and enter the manifolds as shunt currents. This first $R_e/2$ resistance that $I_T$ must pass through is combined with the last $R_e/2$ resistance that $I_T$ must pass through to exit the last cell via the terminal cathode and is represented as the right most $R_e$ resistor in Fig. 2. Also, the open-circuit potential of the cell that the total current passes through when entering the solution through the terminal anode and leaving the solution via the terminal cathode is represented in the circuit analog model as the right most $V_0$ in Fig. 2. Note that in the analog circuit model, the manifolds are assumed to be electrically insulated from ground and are themselves nonconducting.

The circuit in Fig. 2 can be simplified by assuming that $R_{t,in}$ and $R_{t,out}$ are in parallel so that an equivalent resistance $R_2$ can be defined for the inlet and outlet tubes as

$$\frac{1}{R_2} = \frac{1}{R_{t,in}} + \frac{1}{R_{t,out}} \quad [1]$$

and, in a like manner, an equivalent resistance $R_3$ can be defined for the inlet and outlet manifold resistances

$$\frac{1}{R_3} = \frac{1}{R_{m,in}} + \frac{1}{R_{m,out}} \quad [2]$$

The resulting simplified circuit is shown in Fig. 3.

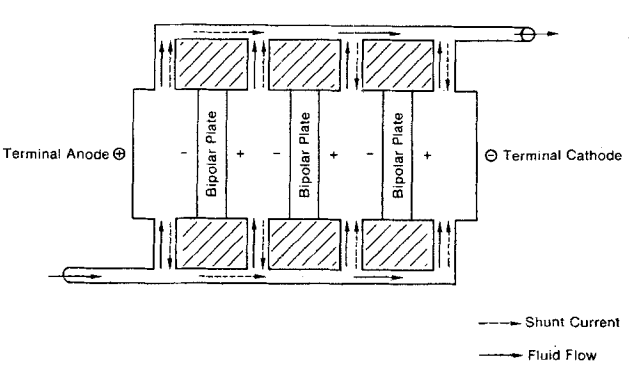


Fig. 1. Schematic of a stack of four undivided bipolar plate cells

*Electrochemical Society Active Member.
**Electrochemical Society Student Member.

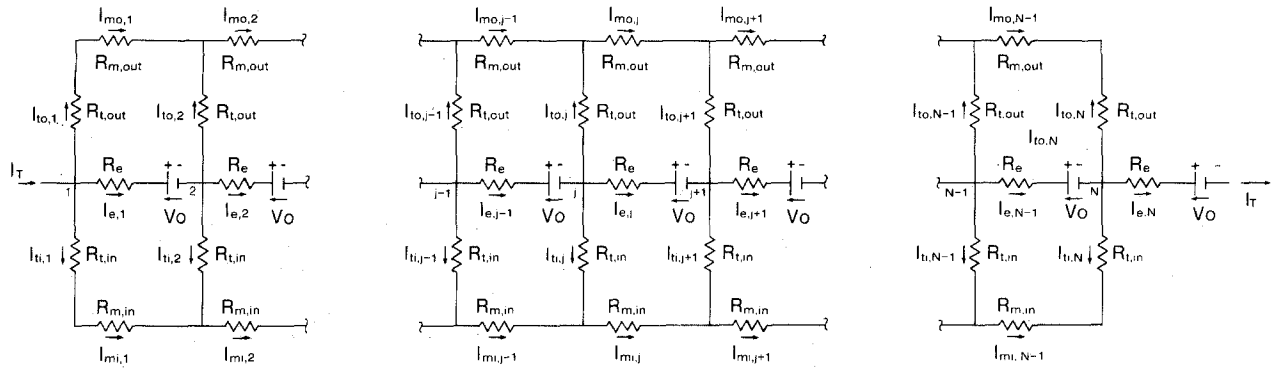

Fig. 2. Circuit analog model for a stack of N undivided bipolar plate cells

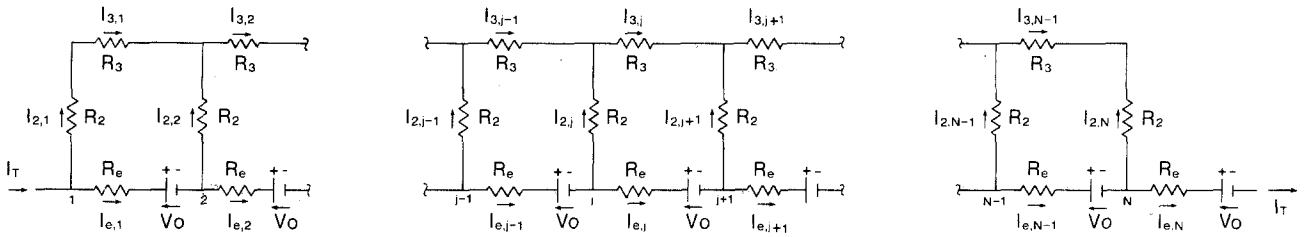

Fig. 3. Simplified form of the circuit shown in Fig. 2

It is worth mentioning at this point that some workers have extended the circuit analog model shown in Fig. 3 to include nonlinear elements to account for the actual current-potential relationship that exists in the cells of interest. Katz (1), for example, added zener diodes to the $R_2$ branches of Fig. 3 and Kuhn and Booth (2) added zener diodes to the $R_e$ branches of Fig. 3 for this purpose. These nonlinear elements will be discussed further below.

Consideration of the circuits in Fig. 2 and 3 reveals that two special cases exist. One of these cases exists when $R_{t,in} >> R_{t,out}$ (or vice versa) and $R_{m,in} >> R_{m,out}$ (or vice versa) and the other exists when $R_{t,in} = R_{t,out}$ and $R_{m,in} = R_{m,out}$. In the first case, the currents in the two circuits in Fig. 2 and 3 are essentially the same (*i.e.*, $I_{to,j} = I_{2j}$ and $I_{mo,j} = I_{3j}$) since current would not enter the lower portion of the circuit in Fig. 2. In the second case, it can be shown that the currents in the branches of the circuit in Fig. 2 are equal to one-half of those in Fig. 3 (*i.e.*, $I_{ci,j} = I_{co,j} = I_{2j}/2$ and $I_{mi,j} = I_{mo,j} = I_{3j}/2$), as expected based on the symmetry of the circuit in Fig. 2. For all other cases, the currents in Fig. 2 can be determined directly (see below), or approximately by using the current obtained from an analysis of the circuit in Fig. 3. That is

$$I_{e,j}\ (\text{Fig. 2}) \cong I_{e,j}\ (\text{Fig. 3}) \quad [3]$$

$$I_{ti,j} \cong \frac{R_2}{R_{t,in}} I_{2,j} \quad [4]$$

$$I_{to,j} \cong \frac{R_2}{R_{t,out}} I_{2,j} \quad [5]$$

$$I_{mi,j} \cong \frac{R_3}{R_{m,in}} I_{3,j} \quad [6]$$

and

$$I_{mo,j} \cong \frac{R_3}{R_{m,out}} I_{3,j} \quad [7]$$

Predictions for the currents in Fig. 3 have been obtained by a variety of methods. One method used by some workers (3-8) consists of writing the finite difference form of the equations for the currents in Fig. 3 (see below) in continuous form. That is, it is assumed that a linear differential equation can be used to replace the finite difference equations for the currents for a large number of cells. The resulting differential equation is then solved by standard methods which yield a solution containing exponential terms. This approach is of limited utility because of the required assumption of a large number of cells. A similar approach has been used recently by Grimes *et al.* (9-13) in which they solve the finite difference equation for the currents in Fig. 3 by using a power law solution technique (9). Unfortunately, neither of these methods can be used easily, if at all, to solve for the currents in a circuit like Fig. 3 with nonlinear elements [see Fig. 5 of Ref. (1), *e.g.*]. Another method for solving for the currents in Fig. 3 consists of using standard matrix techniques to solve the governing finite difference equations, as discussed in Ref. (1), (2), (14), and (15). These standard matrix techniques can be used to solve approximately for currents in circuits which have nonlinear elements (1). The method used by Katz (1) is only approximate because he uses a linear current-potential relationship for cell j and then uses iteration to find the proper slope and intercept values for the linear polarization relationships for cell j. The treatment of the nonlinearities by Kuhn and Booth (2) is based on a similar method, but their method is, unfortunately, based on a software package that is not widely available. A simple, direct method for treating circuits with nonlinear current-potential relationships is presented below.

As shown in Eq. [3]-[7], once values for the currents in Fig. 3 are known, they can be used to predict approximately the currents in Fig. 2. If more accurate values of the currents in Fig. 2 are of interest, they can be obtained

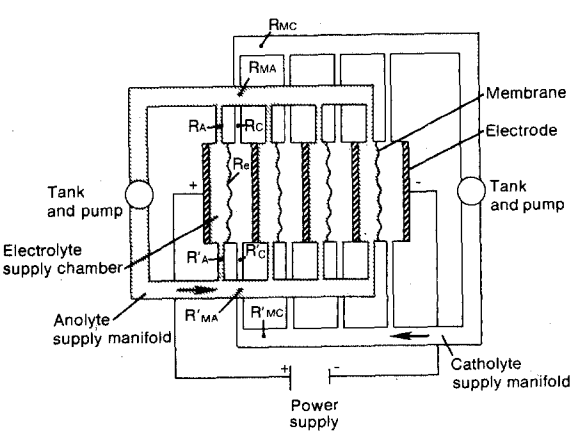


Fig. 4. Schematic of a stack of divided bipolar plate cells

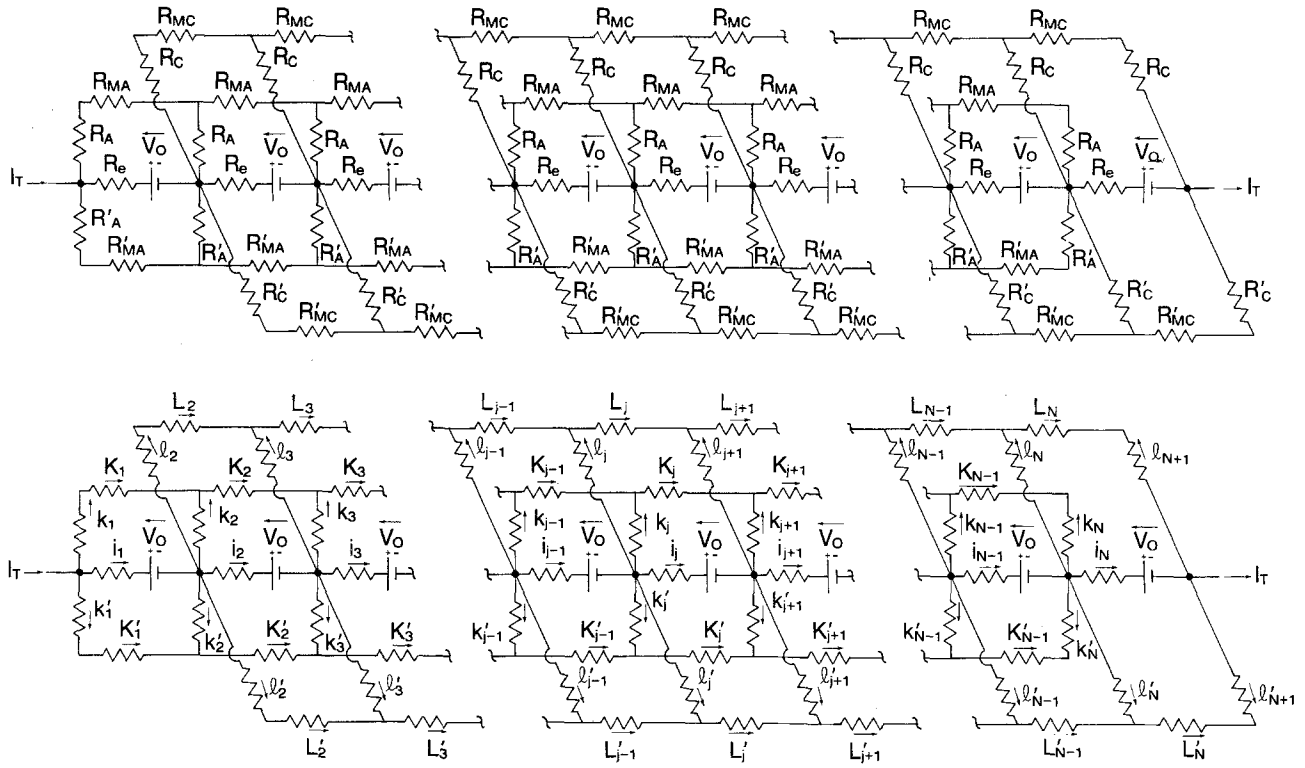

Fig. 5. Circuit analog model of a stack of N divided bipolar plate cells

by using the method presented here or standard matrix methods as shown by Rousar and Cezner (16). Another approximate method of determining the currents in Fig. 2 was presented by Burnett and Danly (17). Their method is approximate because they assume that $R_{m,in} = R_{m,out} = 0$ which leads to a simple solution but unfortunately yields an incorrect dependence of the fractional amount of current loss due to shunt currents on the number of cells, as shown first by Farnum (18) and discussed further below.

*Divided cells.*—A schematic of a stack of divided bipolar plate cells is shown in Fig. 4. This schematic, which is similar to that presented by Prokopius (19), can be used to formulate the circuit analog model shown in Fig. 5, which is similar to that presented by Prokopius and by Kaminski and Savinell (20). This model is based on the conceptualization that the stack consists of a series of compartments for the terminal anode, bipolar plates, and the terminal cathode, and that these compartments are separated by ion exchange membranes, for example. Also, note that only the inlet and outlet anolyte streams are connected to the terminal anode compartment and only the inlet and outlet streams of the catholyte are connected to the terminal cathode compartment. The total current enters the stack by overcoming the anodic portion of the open-circuit potential of the cell potential which, as before, is lumped with the cathodic portion of the open-circuit cell potential and is shown as the right most $V_o$ in Fig. 5. Next, some of the total current leaves the terminal anode compartment through both the inlet and outlet anolyte tubes and the rest of the total current passes through the resistance due to the first membrane. It is assumed for simplicity in this model that the resistances of the electrolyte and the bipolar plates in the main current path are negligible relative to the resistance of the membrane ($R_e$). This means that no real cell dimensions (electrode gap, bipolar plate thickness, etc.) have been included in this model so that the branch currents through the inlet and outlet tubes effectively meet at a central node point as shown in Fig. 5. However, the tube and manifold resistances can be determined in the usual way (17) by using tube and manifold dimensions and the specific resistivity of the electrolyte in them. Once the majority of the current passes through the first membrane, it enters the first bipolar plate compartment and overcomes the open-circuit cell potential. Next, a portion of the current leaves the compartment via the inlet and outlet tubes of both the anolyte and catholyte streams, as shown as node point number 2 in Fig. 5. The current continues through the stack in this manner until passing through the last membrane and entering the terminal cathode compartment. Here the current can enter the compartment from the catholyte inlet and outlet tubes only, as represented by the last node point in Fig. 5.

Methods for predicting the currents in Fig. 5 with symmetrical resistances (*i.e.*, $R_A = R'_A$, etc.) have been presented by Prokopius (19) and Kaminski and Savinell (20). The method used by Prokopius is a standard matrix method, which is probably not suitable for use with a large number of cells with nonlinear circuit elements and unsymmetrical resistances. His method was not considered in depth here because of a lack of sufficient detail in his report. The method presented by Kaminski and Savinell [see also Kaminski (21)] is computationally more efficient than that presented by Prokopius but, unfortunately, it does not appear that their method can be extended easily, if at all, to treat circuits with nonsymmetrical resistances and nonlinear circuit elements.

The currents in Fig. 5 have also been predicted in an approximate manner by Burnett and Danly (17). They determined the fraction of current loss due to shunt currents for the anolyte side using a simplified form of the circuit in Fig. 2 and did the same thing for the catholyte side and added the two together to obtain the total loss due to shunt currents.

Finally, it should be mentioned here that others (22-24) have presented methods for predicting shunt currents based on solving Laplace's equation or a combination of Laplace's equation and a circuit analog model (25), and others (26-28) have presented papers that deal mostly with the experimental aspects of shunt currents.

## Solution Technique

The currents in Fig. 2, 3, and 5 can be obtained by using the concept that all of the currents in a particular branch (or branches) of the circuit can be treated as unknown currents at a particular node point on the central branch of the circuit. That is, for example, the unknown currents $I_{e,j}$, $I_{2,j}$, and $I_{3,j}$ in Fig. 3 can be assumed to exist at node point j. The three governing finite difference equations that apply for these currents can be obtained from Kir-

choff's node and loop rules as follows

$$\text{for } 1 < j < N$$

$$I_{e,j-1} = I_{e,j} + I_{2,j} \quad [8]$$

$$I_{3,j-1} + I_{2,j} = I_{3,j} \quad [9]$$

$$V_o = -R_e I_{e,j} + R_2 I_{2,j} + R_3 I_{3,j} - R_2 I_{2,j+1} \quad [10]$$

This same concept can be applied to the first and last node points

$$\text{at } j = 1$$

$$I_T = I_{e,1} + I_{2,1} \quad [11]$$

$$I_{2,1} = I_{3,1} \quad [12]$$

$$V_o = -R_e I_{e,1} + R_2 I_{2,1} + R_3 I_{3,1} - R_2 I_{2,2} \quad [13]$$

and

$$\text{at } j = N$$

$$I_{e,N-1} = I_{e,N} + I_{2,N} \quad [14]$$

$$I_{3,N-1} = -I_{2,N} \quad [15]$$

$$I_{3,N} = 0 \quad [16]$$

Values for the currents $I_{e,j}$, $I_{2,j}$, and $I_{3,j}$ can be determined by using Newman's BAND(J) subroutine (29-31) to solve Eq. [8]-[16] once values have been specified for $I_T$, $V_o$, $R_e$, $R_2$, $R_3$, and $N$, as discussed in Appendix A of Ref. (32). This same conceptualization of writing the governing equations for the local unknown branch currents as if they all existed at node point j on the central branch of the circuit can also be applied to the currents in Fig. 2 and 5, as discussed in Appendix B and C of Ref. (32). It is worth noting that this means that five and nine unknown currents exist at each central node point for the circuit analogs presented in Fig. 2 and 5, respectively. Newman's BAND(J) subroutine is ideally suited to solve this type of problem for a large number of cells (>50) because it requires less computer storage and less computer time than standard matrix techniques. This method is referred to here as the exact or BAND(J) method.

This BAND(J) method can be extended easily to treat nonlinear circuit elements. That is, for example, the circuit elements $V_o$ and $R_e$ in Fig. 3 could be removed and replaced by a zener diode placed in the circuit such that the direction of current flow would be the same as that shown for $V_o$. The current-potential relationship for such an element might be represented by a third-order polynominal as follows

$$V_j = a_1 + a_2 I_{e,j} + a_3 I_{e,j}^2 + a_4 I_{e,j}^3 \quad [17]$$

which reduces to the previously used linear current-potential relationship if $a_1 = V_o$, $a_2 = R_e$, and $a_3 = a_4 = 0$. The procedure for using Eq. [17] in the exact method consists of replacing $V_o + R_e I_{e,j}$ in Eq. [10] and [13] by the right-hand side of Eq. [17] as discussed further in Appendix A of Ref. (32). Other nonlinear elements could be added to the circuit in Fig. 3 (or other circuit analog models) and handled in a similar manner.

## Results and Discussion

*Undivided cells.*—Table I presents values for the currents in Fig. 2 for a battery case presented by Kaminski (21) obtained by both the exact method and the approximate method according to Eq. [3]-[7], with $I_{e,j}$, $I_{2,j}$, and $I_{3,j}$ obtained by the exact method. The values obtained for the currents in Fig. 2 using the exact method are the same as those obtained by Kaminski (21), whereas the approximate values are accurate to within about 1% or less except for the manifold currents which disagree by as much as 9%. However, this larger difference in the manifold currents is to be expected due to the additive nature of the manifold currents.

The exact method of calculating the currents in Fig. 2 can also be used to calculate the fraction of the total current lost due to shunt currents as defined by Burnett and Danly (17)

$$\Psi = \frac{NI_T - \sum_{j=1}^{N} I_{e,j}}{NI_T} \quad [18]$$

Table II presents a comparison of the $\Psi$ values obtained

**Table I. Comparison of the exact[a] to the approximate[b] method for calculating the currents in Fig. 2**

Input parameters[c]

$I_T = 0.1\text{A}$, $N = 11$, $V_o = -1.0\text{V}$, $R_e = 3\Omega$

$R_{t,in} = 1200\Omega$, $R_{t,out} = 1000\Omega$, $R_{m,in} = 6\Omega$, $R_{m,out} = 4\Omega$

Results

| Method | Cell number (j) | $10^1 \times I_{e,j}$(A) | $10^3 \times I_{ti,j}$(A) | $10^3 \times I_{to,j}$(A) | $10^3 \times I_{mi,j}$(A) | $10^3 \times I_{mo,j}$(A) |
|---|---|---|---|---|---|---|
| Exact | 1 | 1.0579 | −2.6171 | −3.1731 | −2.6171 | −3.1731 |
| Exact | 2 | 1.1035 | −2.0614 | −2.5031 | −4.6785 | −5.6762 |
| Exact | 3 | 1.1374 | −1.5273 | −1.8569 | −6.2058 | −7.5331 |
| Exact | 4 | 1.1598 | −1.0093 | −1.2283 | −7.2151 | −8.7614 |
| Exact | 5 | 1.1709 | −0.50202 | −0.61124 | −7.7171 | −9.3727 |
| Exact | 6 | 1.1709 | 0.0000 | 0.0000 | −7.7171 | −9.3727 |
| Exact | 7 | 1.1598 | 0.50202 | 0.61124 | −7.2151 | −8.7614 |
| Exact | 8 | 1.1374 | 1.0093 | 1.2283 | −6.2058 | −7.5331 |
| Exact | 9 | 1.1035 | 1.5273 | 1.8569 | −4.6785 | −5.6762 |
| Exact | 10 | 1.0579 | 2.0614 | 2.5031 | −2.6171 | −3.1731 |
| Exact | 11 | 1.0000 | 2.6171 | 3.1731 | 0.0000 | 0.0000 |
| Approximate | 1 | 1.0579 | −2.6332 | −3.1599 | −2.3172 | −3.4759 |
| Approximate | 2 | 1.1036 | −2.0760 | −2.4911 | −4.1441 | −6.2161 |
| Approximate | 3 | 1.1375 | −1.5393 | −1.8471 | −5.4986 | −8.2480 |
| Approximate | 4 | 1.1599 | −1.0178 | −1.2213 | −6.3943 | −9.5914 |
| Approximate | 5 | 1.1710 | −0.50638 | −0.60766 | −6.8399 | −10.2599 |
| Approximate | 6 | 1.1710 | 0.0000 | 0.0000 | −6.8399 | −10.2599 |
| Approximate | 7 | 1.1599 | 0.50638 | 0.60766 | −6.3943 | −9.5914 |
| Approximate | 8 | 1.1375 | 1.0178 | 1.2213 | −5.4986 | −8.2480 |
| Approximate | 9 | 1.1036 | 1.5393 | 1.8471 | −4.1441 | −6.2161 |
| Approximate | 10 | 1.0579 | 2.0760 | 2.4911 | −2.3172 | −3.4759 |
| Approximate | 11 | 1.0000 | 2.6332 | 3.1599 | 0.0000 | 0.0000 |

[a] The equations for the exact method are presented in Appendix B of Ref. (32).
[b] Currents obtained according to Eq. [3]-[7].
[c] This case and the answers are the same as those presented in Table I of Kaminski (21).

Table II. Comparison of $\Psi$ values obtained from the exact[a] method to that obtained by Burnett and Danly (17)

Fixed input parameters (anolyte only)

$I_T = 3000A$, $N = 40$, $V_o = 10V$

$R_{t,in} = 34\Omega$, $R_{t,out} = 39\Omega$

| $\Psi$ (Anolyte) | | | | | |
|---|---|---|---|---|---|
| Exact[a] | Burnett and Danly (17) | $R_e$ ($\Omega$) | $R_{m,in}$ ($\Omega$) | $R_{m,out}$ ($\Omega$) | Case[d] |
| 0.0481 | 0.0248 | 0.00333[b] | 0 | 0 | A |
| 0.0248 | 0.0248 | 0 | 0 | 0 | B |
| 0.0440 | 0.0248 | 0.00333[b] | 0.02[c] | 0.02[c] | C |
| 0.0227 | 0.0248 | 0 | 0.02 | 0.02 | D |
| 0.0840 | 0.0248 | 0.01 | 0.02 | 0.02 | E |

[a] The equations for the exact method are presented in Appendix B of Ref. (32).
[b] Obtained by dividing $V_o$ by $I_T$.
[c] Arbitrarily selected value.
[d] Cases A, B, and C, are presented in Fig. 6 for different values of $N$.

according to the exact method with various resistance values and those obtained by Burnett and Danly (17) for the anolyte of their example case. Inspection of the $\Psi$ values in Table II reveals that the exact method yields significantly different values from those presented by Burnett and Danly (17) except for the case where $R_e = R_{m,in} = R_{m,out} = 0$. Figure 6 shows how $\Psi$ depends on $N$ for three of the cases (A, B, and C) presented in Table II. Clearly, $\Psi$ depends on $N$, but not as $N^2$, as reported by Burnett and Danly (17) unless $R_{m,in} = R_{m,out} = 0$. Note that, if the manifolds offer resistance to the passage of current, $\Psi$ will approach a constant, as pointed out by Farnum (18) and illustrated in Fig. 6 by case C. Further consideration of Table II reveals that the dependence of $\Psi$ on $R_e$ is significant (cf. cases C, D, and E) and should not be ignored, as mentioned earlier by Kuhn and Booth (2).

*Nonlinear circuit elements.*—The effect of a nonlinear current-potential relationship can be demonstrated by replacing $R_e$ and $V_o$ in Fig. 3 with a zener diode with current passing in the same direction as induced by $V_o$ and with the current-potential relationship given by Eq. [17]. The linear and nonlinear model predictions of the shunt current leaving cell number 1 ($I_{2,1}$) can be compared by

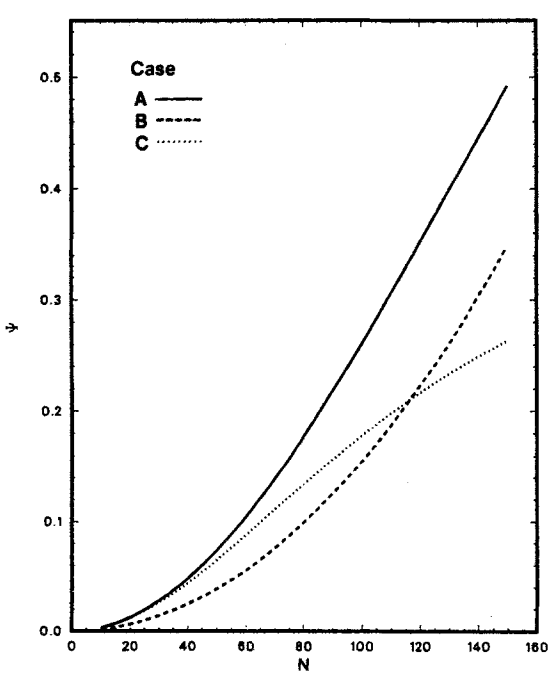


Fig. 6. Comparison of methods for calculating the fraction of current bypassed (see Table II for the parameters for cases A, B, and C.)

Table III. Comparison of predicted values for $I_{2,1}$ (Fig. 3) for linear and nonlinear current-potential relationships for three values of $R_2$

Fixed input parameters

$a_1 = V_o = 1.95V$, $N = 20$, $I_T = 8000A$, $R_3 = 0.01\Omega$,

$R_e$[a] $= 1.31 \times 10^{-4}\Omega$, $a_2 = 2.037 \times 10^{-4}\Omega$,

$a_3 = -1.045 \times 10^{-8}\ \Omega/A$, $a_4 = 2.148 \times 10^{-13}\ \Omega/A^2$

| $I_{2,1}$ (A) | | | Variable parameter |
|---|---|---|---|
| Linear | Nonlinear | % Difference[b] | $R_2$ ($\Omega$) |
| 2.75 | 2.47 | 11.3 | 10.0 |
| 5.32 | 4.78 | 11.3 | 5.0 |
| 21.3 | 19.2 | 10.9 | 1.0 |

[a] Obtained from Eq. [33] with $V_{cell} = 3.0V$.
[b] Relative to the nonlinear values.

using one of two methods for approximating Eq. [17]. The first method is to determine the value of $R_e$ based on the cell potential for a single cell measured at $I_T$. That is, by setting $j = N = 1$, $V_1 = V_{cell}$, $a_1 = V_o$, $a_2 = R_e$, $I_{1,1} = I_T$, $a_3 = 0$, and $a_4 = 0$, Eq. [17] becomes

$$R_e = \frac{V_{cell} - V_o}{I_T} \quad [19]$$

which, by using known values for $V_{cell}$, $V_o$, and $I_T$, yields a value for $R_e$ that is assumed to apply at and near the set value of $I_T$. The second method consists of using the derivative of Eq. [17] evaluated at $I_T$ to determine a value for $V_o$ according to

$$V_o = V_{cell} - I_T \frac{dV_j}{dI_{1,j}}\bigg|_{I_{1,j} = I_T} \quad [20]$$

That is, at a set value of $I_T$, Eq. [17] with known values of $a_1 - a_4$ is used to obtain a value for the derivative appearing in Eq. [20]. This value of the derivative is equated to $R_e$ and is used in Eq. [20] to determine $V_o$ for use in the linear approximation of $V_j$ ($V_j = V_o + R_e I_{e,j}$). The first method is used here, but both methods yield essentially the same results. Table III presents the predicted tube current out of the first cell ($I_{2,1}$) for the linear and nonlinear models with three different values of $R_2$. Comparison of the values for $I_{2,1}$ presented in Table III reveals that the nonlinear circuit element approach leads to a smaller predicted shunt current ($\approx$ 10% less) for cell number 1,

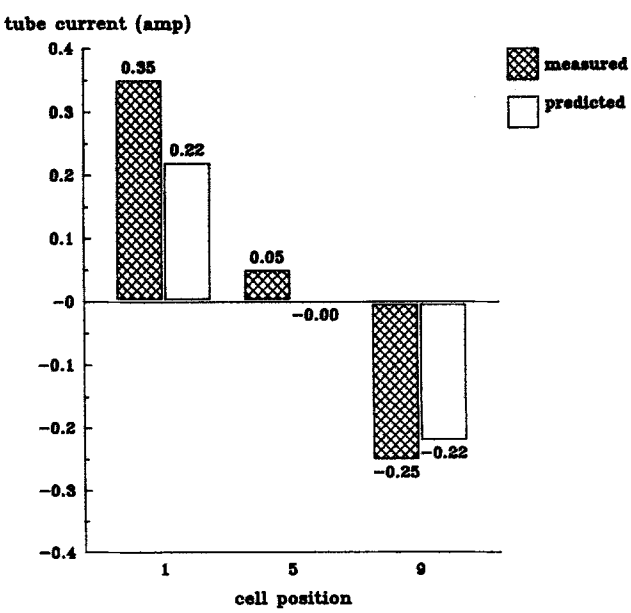


Fig. 7. Comparison of measured vs. predicted anolyte inlet tube shunt currents.

**Table IV. Predicted currents for the divided cell model based on Fig. 5 with symmetrical resistances[a]**

Fixed input parameters

$N = 3$, $I_T = 0.5A$, $V_o = -1.5V$, $R_e = 1\Omega$,
$R_A = R'_A = 5000\Omega$, $R_C = R'_C = 400\Omega$,
$R_{MA} = R'_{MA} = 10\Omega$, $R_{MC} = R'_{MC} = 5\Omega$

Selected predicted currents

| $j$ | $i_j$ (A) | $k'_j$ (A) | $l'_j$ (A) | $k_j$ (A) | $l_j$ (A) |
|---|---|---|---|---|---|
| 1 | 0.5004 | $-1.992 \times 10^{-4}$ | 0.0000 | $-1.992 \times 10^{-4}$ | 0.0000 |
| 2 | 0.5053 | $3.273 \times 10^{-7}$ | $-2.456 \times 10^{-3}$ | $3.273 \times 10^{-7}$ | $-2.456 \times 10^{-3}$ |
| 3 | 0.5049 | $1.989 \times 10^{-4}$ | $-3.295 \times 10^{-7}$ | $1.989 \times 10^{-4}$ | $-3.295 \times 10^{-6}$ |
| 4 | 0.5000 | 0.0000 | $2.457 \times 10^{-3}$ | 0.0000 | $2.457 \times 10^{-3}$ |

[a] Same case as that presented by Kaminski (21) in his Table III.

**Table V. Predicted currents for the divided cell model based on Fig. 5 with unsymmetrical resistances**

Fixed input parameters

$N = 3$, $I_T = 0.5A$, $V_o = -1.5V$, $R_e = 1\Omega$,
$R_A = 5000\Omega$, $R'_A = 2500\Omega$, $R_C = 400\Omega$, $R'_C = 200\Omega$,
$R_{MA} = 10\Omega$, $R'_{MA} = 5\Omega$, $R_{MC} = 5\Omega$, $R'_{MC} = 2.5\Omega$

Selected predicted currents

| $j$ | $i_j$ (A) | $k'_j$ (A) | $l'_j$ (A) | $k_j$ (A) | $l_j$ (A) |
|---|---|---|---|---|---|
| 1 | 0.5006 | $-3.980 \times 10^{-4}$ | 0.0000 | $-1.990 \times 10^{-4}$ | 0.0000 |
| 2 | 0.5080 | $9.792 \times 10^{-7}$ | $-4.900 \times 10^{-3}$ | $4.896 \times 10^{-7}$ | $-2.450 \times 10^{-3}$ |
| 3 | 0.5074 | $3.970 \times 10^{-4}$ | $-9.859 \times 10^{-7}$ | $1.985 \times 10^{-4}$ | $-4.930 \times 10^{-7}$ |
| 4 | 0.5000 | 0.0000 | $4.901 \times 10^{-3}$ | 0.0000 | $2.451 \times 10^{-3}$ |

**Table VI. Predicted currents for a stack of bipolar plate, membrane chlor-alkali cells**

Fixed input parameters

$N = 9$, $I_T = 20770A$, $V_o = -1.9607V$, $R_e = 6.234 \times 10^{-5}\Omega$,
$R_A = 34.5\Omega$, $R'_A = 58.8\Omega$, $R_C = 15.6\Omega$, $R'_C = 26.6\Omega$,
$R_{MA} = 6.9 \times 10^{-2}\Omega$, $R'_{MA} = 6.9 \times 10^{-2}\Omega$, $R_{MC} = 3.14 \times 10^{-2}\Omega$, $R'_{MC} = 3.14 \times 10^{-2}\Omega$

Selected predicted currents

| Cell number $j$ | Internal cell current $i_j$ (A) | Inlet tube currents: Anolyte $k'_j$ (A) | Inlet tube currents: Catholyte $l'_j$ (A) | Outlet tube currents: Anolyte $k_j$ (A) | Outlet tube currents: Catholyte $l_j$ (A) |
|---|---|---|---|---|---|
| 1 | 20769.40862 | 0.219520 | 0 | 0.371858 | 0 |
| 2 | 20767.65846 | 0.164412 | 0.485223 | 0.278240 | 0.822290 |
| 3 | 20766.38509 | 0.109499 | 0.363414 | 0.185182 | 0.615268 |
| 4 | 20765.58635 | 0.054717 | 0.242037 | 0.092497 | 0.409490 |
| 5 | 20765.26087 | −0.000001 | 0.120947 | −0.000002 | 0.204540 |
| 6 | 20765.40809 | −0.054719 | 0.000001 | −0.092500 | 0.000002 |
| 7 | 20766.02825 | −0.109500 | −0.120945 | −0.185184 | −0.204536 |
| 8 | 20767.12243 | −0.164411 | −0.242036 | −0.278239 | −0.409489 |
| 9 | 20768.69248 | −0.219516 | −0.363414 | −0.371852 | −0.615270 |
| | 20770.00000 | 0 | −0.485226 | 0 | −0.822295 |

Fraction of current bypassed ($\Psi$) = $1.522 \times 10^{-4}$.

where the highest possible shunt current would be expected to exist.

*Divided cells.*—Results are presented here for two cases. The first case is for a battery stack and the second case is for stacks of bipolar plate, membrane chlor-alkali cells. Table IV presents the currents calculated for the circuit shown in Fig. 5 for the same battery case as that presented by Kaminski (21) in his Table III. Comparison of the values presented here to those presented by Kaminski reveals that the two different methods yield essentially the same results, as expected. Table V presents the results obtained when the symmetrical resistances in Table IV are made unsymmetrical by dividing $R'_A$, $R'_C$, $R'_{MA}$, and $R'_{MC}$ by 2. Comparison of the currents presented in Table IV and V reveals that they differ significantly. The degree of importance of this difference depends, of course, on how much difference exists between $R_A$ and $R'_A$, etc. Unfortunately, there does not appear to be a simple parameter to predict quantitatively the importance of unsymmetrical resistances.

Table VI presents the parameter values and the predicted currents obtained for a stack of nine bipolar plate, membrane chlor-alkali cells. The results show that it is possible to predict the currents in each of the connecting tubes to the cells. The values predicted for some of these tube currents were verified qualitatively with a clip-on Hall-effect (inductive) ammeter as shown in Fig. 7 and 8. The measured values shown in these figures are only qualitatively significant because the accuracy of the ammeter apparatus used was only ± 0.1A, due to the sensitivity limit of the strength of the inductive field.

The effect of increasing the number of cells on the predicted maximum catholyte outlet tube current is shown in Fig. 9 for full and half-full outlet tubes and manifolds (half-full values obtained by doubling the values for $R_A$, $R_C$, $R_{MA}$, and $R_{MC}$ in Table VI). Finally, Fig. 10 shows the effect on the percent bypass current of increasing the number of cells. Figures 9 and 10 both illustrate the importance of the number of cells and the ability of the model to account for the fact that outlet tubes and mani-

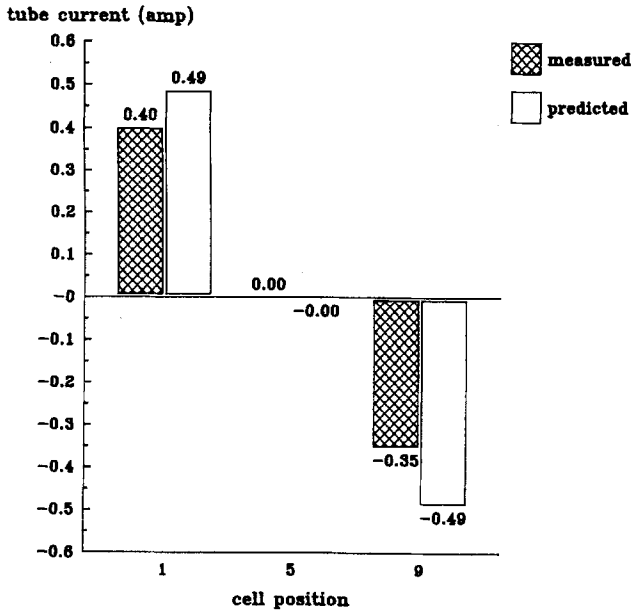


Fig. 8. Comparison of measured *vs.* predicted catholyte inlet tube shunt currents.

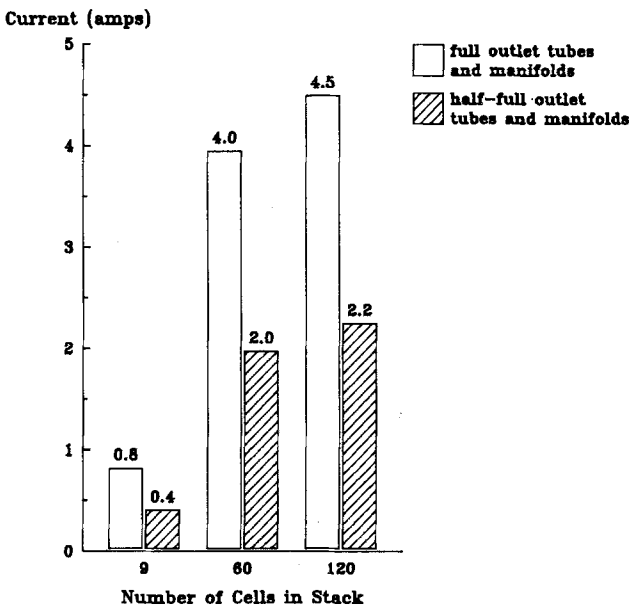


Fig. 9. Maximum predicted shunt current for catholyte outlet tube

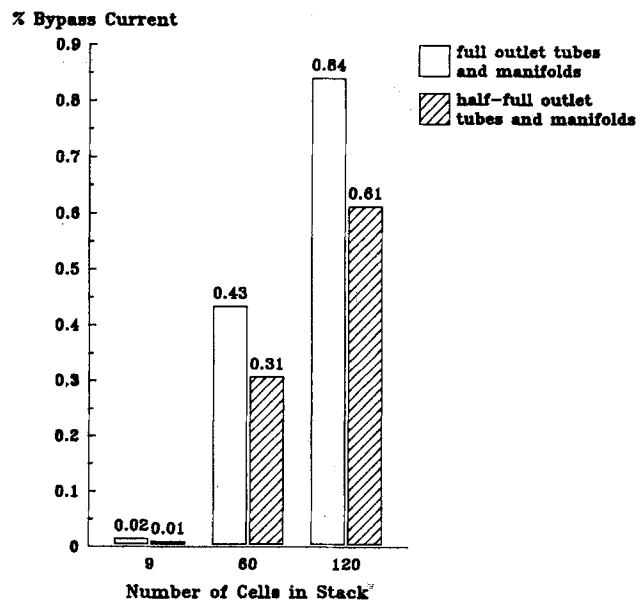


Fig. 10. Predicted percent bypass current

folds, for example, may be only half-full due to presence of product gases. It should be noted in closing that an interesting approach to reduce the shunt currents in chlor-alkali cells has been presented recently by Mataga and Takenaka (33). Their approach consists of inserting the inlet and outlet tubes into the cells.

## Conclusions

Shunt currents in stacks of either divided or undivided bipolar plate cells with or without nonlinear current-potential relationships can be predicted easily and efficiently by using circuit analog models with or without symmetrical resistances, Kirchoff's node and loop rules, and Newman's BAND(J) subroutine. The expression presented by Burnett and Danly (17) for the fractional amount of current lost due to shunt currents is correct only if $R_e = R_{m,in} = R_{m,out} = 0$. It is important to include nonsymmetrical resistances, if they exist, in the circuit analog models because the predicted tube currents depend significantly on the values of all other resistances for a large number of cells.

Finally, it should be noted that this method of predicting shunt currents based on circuit analog models is inherently limited because of the assumptions of lumped resistances and should be used with caution.

## Acknowledgment

The authors acknowledge gratefully that this work was supported by the Texas Applied Science and Technology Laboratories of Dow Chemical USA.

Manuscript submitted June 3, 1985; revised manuscript received Nov. 20, 1985.

*Dow Chemical USA assisted in meeting the publication costs of this article.*

## REFERENCES

1. M. Katz, *This Journal*, **125**, 515 (1978).
2. A. T. Kuhn and J. S. Booth, *J. Appl. Electrochem.*, **10**, 233 (1980).
3. V. B. Kogan and R. R. Ousepyan, *Khim. Prom.*, **8**, 463 (1954).
4. A. S. Bogoslovskii, *Tsvetnye Metally.*, **29** (4), 57 (1956).
5. O. S. Ksenzhek and N. D. Koshel, *Elektrokhimiya*, **7**, 353 (1971).
6. V. A. Onishchuk, *ibid.*, **8**, 698 (1972).
7. B. P. Nestewrov, G. A. Kamzelev, V. P. Gerasimenko, and N. V. Korovin, *ibid.*, **9**, 1154 (1973).
8. W. Thiele, M. Schlieff, and H. Matschiner, *Electrochim. Acta*, **26**, 1005 (1981).
9. M. Zahn, P. Grimes, and R. Bellows, U.S. Pat. 4,197,169 (1980).
10. P. G. Grimes, M. Zahn, and R. J. Bellows, U.S. Pat. 4,312,735 (1982).
11. P. G. Grimes, U.S. Pat. 4,377,445 (1983).
12. P. G. Grimes, R. J. Bellows, and M. Zahn, in "Electrochemical Cell Design," R. E. White, Editor, p. 259, Plenum Publishing Co., New York (1984).
13. P. G. Grimes and R. Bellows, *ibid.*, p. 277.
14. I. Rousar, *This Journal*, **116**, 676 (1969).
15. R. F. Savinell and R. L. Dotson, "Fundamentals and Principles of Electrochemical Engineering," AIChE Today Series, American Institute of Chemical Engineers, New York (1981).
16. I. Rousar and V. Cezner, *This Journal*, **121**, 648 (1974).
17. J. C. Burnett and D. E. Danly, in Symposium on Electro-Organic Synthesis Technology, American Institute of Chemical Engineers, New York (1978).
18. A. S. Farnum *et al.*, Dow CRI Report (1982).
19. P. R. Prokopius, NASA TM X-3359 (1976).
20. E. A. Kaminski and R. F. Savinell, *This Journal*, **130**, 1103 (1983).
21. E. A. Kaminski, M. S. Thesis, University of Akron, Akron, OH (1983).
22. J. B. Riggs, Abstract 123, p. 333, The Electrochemical Society Extended Abstracts, Vol. 80-2, Hollywood, FL, Oct. 5-10, 1980.
23. J. A. Holmes and R. E. White, in "Electrochemical Cell Design," R. E. White, Editor, p. 311, Plenum Publishing Co., New York (1984).
24. D. E. Stephens, S. D. Mott, and M. Shabrang, Abstract 265, p. 683, The Electrochemical Society Extended Abstracts, Vol. 79-1, Boston, MA, May 6-11, 1979.
25. S. Szpak, C. J. Gabriel, and J. R. Driscoll, *This Journal*, **131**, 1996 (1984).
26. L. M. Yakimenkov, F. Z. Serebryanskii, and L. I.

Korneev, *Zhurmal Prikladnoi Khimii*, **44**, 1290 (1971).
27. C. J. H. King and D. E. Danly, Abstract 392, p. 648, The Electrochemical Society Extended Abstracts, Vol. 82-1, Montreal, Que., Canada, May 9-14, 1982.
28. V. I. Ginzburg, E. F. Ryabou, and V. L. Kubasou, *The Soviet Chemical Industry*, **16**, 81 (1984).
29. J. S. Newman, "Electrochemical Systems," Prentice-Hall, Inc., Englewood Cliffs, NJ (1973).
30. R. E. White, *Ind. Eng. Chem., Fundam.*, **17**, 367 (1978).
31. J. Van Zee, G. Kleine, R. E. White, and J. Newman, in "Electrochemical Cell Design," R. E. White, Editor, p. 377, Plenum Publishing Co., New York (1984).
32. R. E. White, H. S. Burney, and R. N. Beaver, in "Modern Chlor-Alkali Technology" Vol. 3, K. Wall, Editor, Ellis Horwood Ltd., Chichester, West Sussex, England, in press.
33. S. Mataga and M. Takenaka, U.S. Pat. 4,465,579 (1984).

# Factors That Affect Uniformity of Plating of Through-Holes in Printed Circuit Boards

## II. Periodic Flow Reversal Through the Holes

**Stanley Middleman**

*Department of AMES/Chemical Engineering, University of California, San Diego, La Jolla, California 92093*

ABSTRACT

A model for the effect of flow on the diffusion-limited plating rate inside a through-hole is presented. Unidirectional flow is of limited use in promoting uniformity. Periodic alternating flow is much more effective. Subject to a number of simplifying assumptions, the model permits estimates of the effects of various parameters on plating uniformity.

In a previous paper (1) we demonstrated that stagnant liquid, trapped in the through-holes of a printed circuit board, gives rise to a diffusion resistance that leads to significant nonuniformity of the deposition rate on the walls of the hole. In commercial electroplating systems, attempts are made to provide agitation of the plating bath so as to promote mass transfer within the holes. Whether this is successful or not depends upon the extent to which agitated liquid can actually be convected into these holes.

In this paper, we examine a mathematical model that relates the degree of nonuniformity to the character of the flow through the hole. In this way, we can establish criteria for the nature of the flow that must be induced in the process in order to achieve a specified level of uniformity. In the third part of this series, we will examine the details of interaction between the agitation in the external bath and the flow induced through the holes.

A primary goal of this investigation is to establish estimates of the degree to which uniformity can be improved through the control of flow through the holes. To this end, we have selected particularly simple conditions which permit analytical solutions to the model equations for convection, diffusion, and reaction. It then becomes relatively easy to examine one specific feature of flow control: periodic flow reversal.

### Model Development

Figure 1 shows the geometry and nomenclature for our model of diffusion, reaction, and flow in a through-hole. We assume that an axial flow exists in the hole, and that the flow is steady in time. We assume, further, that the velocity field is fully developed everywhere beyond the entrance, $z = 0$. We will assess the validity and implications of these assumptions later.

The convective diffusion equation, under these assumptions, may be written as (2)

$$u(r)\frac{\partial C}{\partial z} = D\frac{1}{r}\frac{\partial}{\partial r}\left(r\frac{\partial C}{\partial r}\right) \qquad [1]$$

We use molar concentration as the composition variable $C$, and consider a single species: the ion that is being plated on the through-hole surface at $r = a$. Likewise, the diffusion coefficient $D$ is that of the ionic species in the plating solution.

It is convenient to nondimensionalize this equation by introducing the hole radius $a$ as a length scale, and the average velocity $U$ as a velocity scale. We may then write Eq. [1] in the form

$$F(\bar{r})\frac{\partial \bar{C}}{\partial \bar{z}} = \frac{1}{\mathrm{Pe}}\left[\frac{1}{\bar{r}}\frac{\partial}{\partial \bar{r}}\left(\bar{r}\frac{\partial \bar{C}}{\partial \bar{r}}\right)\right] \qquad [2]$$

where

$$\bar{r} = r/a \qquad \bar{z} = z/a \qquad \bar{C} = C/C_b$$

and the Peclet number is defined as

$$\mathrm{Pe} = 2\,a\,U/D \qquad [3]$$

In Eq. [2], the coefficient $F(\bar{r})$ is the dimensionless velocity, which we have written as

$$F(\bar{r}) = \frac{1}{2}\frac{u(\bar{r})}{U} = \frac{1}{2}\bar{u}(\bar{r}) \qquad [4]$$

We will later have to specify the form of $F(\bar{r})$ if we wish to solve Eq. [2].

We note that the axial diffusion term has been neglected in Eq. [1] (and Eq. [2]). This is usually regarded as a good assumption for large Peclet number, say Pe > 100 (3).

We examine boundary conditions before proceeding further. At the entrance to the hole, we impose the boundary condition that the concentration is that of the fluid external to the hole, or

$$\bar{C} = 1 \qquad \text{at} \qquad \bar{z} = 0 \qquad [5]$$

We have assumed axial symmetry, so that a boundary condition on the hole axis is

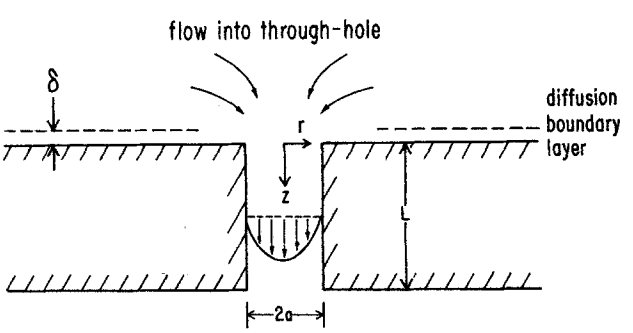


Fig. 1. Definition sketch for mathematical model